Pergamon

Acta Materialia 50 (2002) 2297–2308

Acta MATERIALIA

www.actamat-journals.com

A mesophase transition in a binary monolayer on a solid surface

Y.F. Gao [a], W. Lu [b], Z. Suo [a,*]

[a] *Mechanical and Aerospace Engineering Department and Princeton Materials Institute, Princeton University, Princeton, NJ 08544, USA*

[b] *Mechanical Engineering Department, University of Michigan, Ann Arbor, MI 48109, USA*

Received 11 May 2001; accepted 1 August 2002

Abstract

On a solid surface, an epitaxial monolayer may separate into phases that self-assemble into patterns on the nanoscale. The self-assembly minimizes the combined free energy of mixing, phase boundary, and elasticity. Our recent numerical simulation has revealed an intriguing mesophase transition. The surface stress is a second-rank tensor and can be anisotropic. Depending on the degree of the anisotropy, the lowest energy stripes can be either parallel to, or at an angle from, a principal axis of the surface stress tensor. This paper further elucidates this transition. We show that the off-axis stripes compromise the elastic energy of the inplane and antiplane deformation. The transition between the along-axis and the off-axis stripes obeys the Landau theory of phase transition of the second kind. The off-axis stripes have two variants by symmetry. A set of the stripes of the same variant forms a colony. The two kinds of colonies organize into a mesoscale herringbone structure. Energy minimization sets an equilibrium size of the individual colony.

Keywords: Self-assembly; Nanostructure

1. Introduction

For a decade experiments have shown that, on solid surfaces, monolayers, when separating into distinct phases, can form various two-dimensional patterns, including periodic stripes, triangular lattices, square lattices and irregular arrangements [1–6]. The feature size of the patterns is on the order 1–100 nm, and is often stable on annealing. Fig. 1 illustrates the phenomenon. The monolayer consists of two atomic species, one of which is often identical to that of the substrate. Regard the monolayer as a binary mixture. The free energy of mixing has two wells at concentrations C_α and C_β, corresponding to the two phases α and β. Why do phases on the solid surface self-assemble into patterns with a certain feature size? Recall that when a bulk two-phase alloy is annealed, allowing atoms to diffuse, the phases will coarsen to reduce the total area of the phase boundary. For a two-phase monolayer on a solid surface, the phase boundaries are lines with excess energy, which also drive phase coarsening. The observed stable feature size suggests that, in addition to the phase coarsening action, a phase refining action must exist [7–17].

When the concentration field on the solid surface

* Corresponding author..
E-mail address: suo@princeton.edu (Z. Suo).

1359-6454/02/$22.00
PII: S1359-6454(02)00056-3

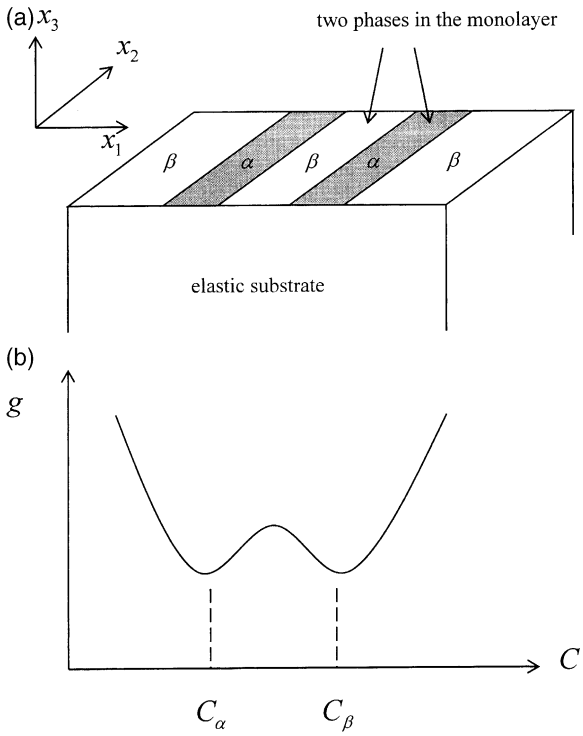

Fig. 1. (a) A schematic of self-assembled binary monolayer on a solid surface. The surface stress of the two phases are different, causing an elastic field in the substrate. (b) The free energy of mixing has two valleys, corresponding to two phases.

is nonuniform, the surface stress is also nonuniform, causing an elastic field inside the substrate. The deformation lowers the total free energy. The smaller the two phases, the better the substrate deformation accommodates the nonuniformity of the surface stress. Consequently, the nonuniform stress drives phase refining [11]. The competition between the phase boundary energy and the elastic energy selects an equilibrium phase size. The morphological change of the phases is effected by atoms diffusing within the monolayer on the surface.

The work of Vanderbilt and co-workers [7–10] highlighted the competing effects of the surface stress and the phase boundary energy. They assumed that the phase boundary was a mathematical line endowed with an excess energy per unit length, and that each phase had a fixed concentration. They then postulated certain phase patterns, such as periodic stripes and triangular lattices, and determined the feature size by minimizing the combined phase boundary energy and elastic energy. Two difficulties arise in models of this kind. First, when the phase boundary is represented as a mathematical line, the concentration and the surface stress jump suddenly across the phase boundary, leading to a singular elastic field. The situation is the same as a line force on the surface of a semi-infinite elastic solid. The elastic energy is unbounded, and the prediction of the equilibrium feature size depends on how the problem is regularized. Second, because the phase patterns are presumed, the true energy minimizer may lie outside the "pool of candidates".

We have recently put forward a continuous phase field model [11–17]. We represent the phase boundary by a concentration gradient, instead of a sudden jump. One may regard this model as a specific way to regularize the problem. The system varies its free energy by two means: the elastic deformation in the substrate, and atomic diffusion in the monolayer. The system attains *mechanical* equilibrium when the free energy variation vanishes with the variation in the elastic displacement, and attains *chemical* equilibrium when the free energy variation vanishes with the variation in the concentration field. The equilibrium phase patterns must attain both mechanical and chemical equilibria. Elastic relaxation is much faster than surface diffusion, so that the system maintains the mechanical equilibrium at all time. For a given concentration field, the equilibrium elastic field is determined by the boundary value problem. The system is not in chemical equilibrium. When the concentration field changes, the change of the free energy defines a thermodynamic force, which, in turn, drives the concentration field change. A nonlinear diffusion equation is derived. Our numerical simulation on the basis of the diffusion equation has revealed diverse phase patterns, such as periodic stripes, serpentine structures, triangular lattices, square lattices and herringbone structures. The phase field model does not presume the pattern type; rather, the diffusion equation leads to the pattern.

The surface stress is a second-rank tensor. We assume that the surface stress $f_{\alpha\beta}$ is linear in the concentration, with $\phi_{\alpha\beta}$ as the slopes. That is, when

the concentration changes by ΔC, the surface stress changes by $\Delta f_{\alpha\beta}=\phi_{\alpha\beta}\Delta C$. The slope tensor $\phi_{\alpha\beta}$ depends on the materials system, and can be measured by the wafer curvature method [3]. Let ϕ_1 and ϕ_2 be the principal values of the ϕ-tensor. The ratio ϕ_2/ϕ_1 measures the anisotropy of the surface stress tensor.

Fig. 2 shows a set of the simulation results. Five values of ϕ_2/ϕ_1 are selected in the simulations. For each simulation the initial concentration fluctuates randomly from the average concentration C_0=0.5. All simulations stop at the same amount of time when the phase patterns become quite stable. A gray scale is adopted to visualize the concentration field. The bright and the dark regions correspond to two phases. The simulation shows three kinds of patterns. In case a, ϕ_2/ϕ_1=1, the surface stress is isotropic, and the phases evolve into a serpentine structure. That is, the overall structure preserves the isotropy during the evolution, and the stripes do not line up in any particular direction. In case b and c, the phases separate and form parallel stripes along the ϕ_2 direction. In case d and e, the phases still separate into alternating stripes, but the stripes are off the principal axis of the ϕ-tensor. Two variants of stripes are permitted by the symmetry. They self-organize into a herringbone structure. It appears that a phase transition occurs with the degree of surface stress anisotropy as a control parameter. We call this a mesophase transition: the mesophases refer to the arrangement of stripes, which themselves are phases of two atomic species. For a given monolayer–substrate system, the surface stress may change with the temperature. In practice, the two kinds of stripe arrangements should be more readily observed in different monolayer–substrate systems.

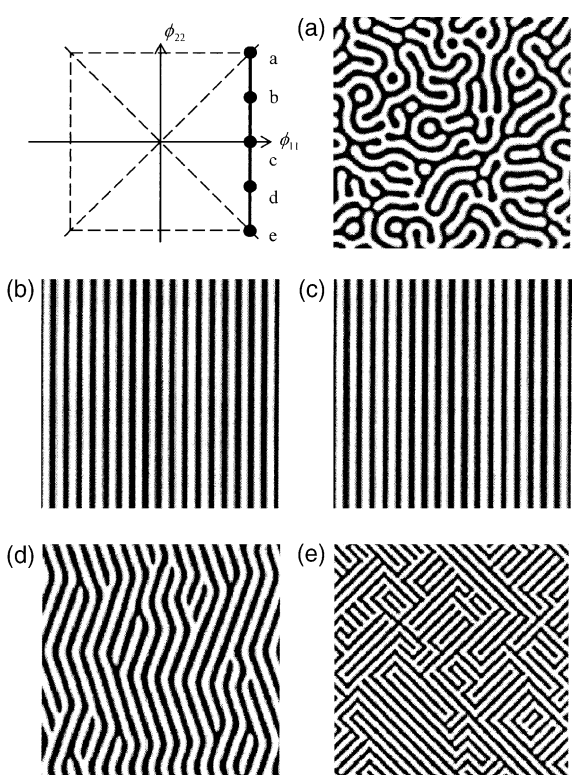

Fig. 2. The results of the kinetic simulation. Five cases have different degrees of surface stress anisotropy. Note the transition from the irregular pattern to straight stripes, and further to herringbone structures.

This paper elucidates this mesophase transition by using an energy minimization method. Section 2 formulates the free energy model. The concentration field attains the mechanical equilibrium by satisfying the exact elasticity solution, and attains the chemical equilibrium by minimizing the free energy. Section 3 assumes that the surface stress is isotropic, and the concentration varies in one direction. We use the Fourier series to represent the concentration field. Energy minimization determines the width of the stripes and the concentration field within the stripes. Section 4 introduces surface stress anisotropy. The concentration field is still assumed to form parallel stripes, but the orientation of the stripes is arbitrary. The lowest energy stripes can be either along or off the principal axis, depending on the degree of surface stress anisotropy. When the stripes are off the principal axis, symmetry dictates that two variants exist. The two variants form a herringbone structure to further reduce the free energy. Section 5 determines the size of the herringbone structure that minimizes the free energy.

2. Mechanical and chemical equilibria

Refer to Fig. 1 again. The substrate is a semi-infinite elastic solid, occupying the half space $x_3<0$. The monolayer coincides with the plane

(x_1,x_2). Let $C(x_1,x_2)$ be the concentration field in the monolayer, and C_0 be the average concentration of the monolayer. We consider the annealing process, in which atoms can relocate within the surface by diffusion. Because no atoms leave or enter the monolayer during annealing, the average concentration remains constant.

Our formulation follows closely the phase field model of bulk crystal due to Cahn and Hilliard [18]. See Chen and Wang [19] for the applications of the phase field model to diverse materials phenomena. The free energy of the system, G, consists of two parts: the bulk elastic energy, and the excess surface energy. We also add a Lagrangian term to fix the average concentration. Write

$$G = \int W\mathrm{d}V + \int \Gamma \mathrm{d}A - \lambda \int (C - C_0)\mathrm{d}A. \tag{1}$$

Here W is the elastic energy density (per unit volume), Γ is the excess surface energy density (per unit area), and λ is the Lagrangian multiplier. The first integral is over the volume of the substrate, and the second and the third integral are over the surface area covered by the monolayer. Both V and A are measured in the undeformed substrate. The Lagrangian multiplier λ may be interpreted as the chemical potential.

Let u_i be the elastic displacement field in the substrate. Latin subscripts run from 1 to 3. The strain tensor ε_ij relates to the displacement as

$$\varepsilon_\mathrm{ij} = \frac{1}{2}(u_\mathrm{i,j} + u_\mathrm{j,i}). \tag{2}$$

Assume that the substrate is elastically isotropic, μ being the shear modulus, and ν Poisson's ratio. The elastic energy density W is quadratic in the strain tensor:

$$W = \mu\left[\varepsilon_\mathrm{ij}\varepsilon_\mathrm{ij} + \frac{\nu}{1-2\nu}(\varepsilon_\mathrm{kk})^2\right]. \tag{3}$$

The repeated subscripts imply the summation convention. The stress tensor relates to the strain tensor as

$$\sigma_\mathrm{ij} = \frac{\partial W}{\partial \varepsilon_\mathrm{ij}} = 2\mu\left(\varepsilon_\mathrm{ij} + \frac{\nu}{1-2\nu}\varepsilon_\mathrm{kk}\delta_\mathrm{ij}\right), \tag{4}$$

where $\delta_\mathrm{ij}=0$ when $i\neq j$, and $\delta_\mathrm{ij}=1$ when $i=j$.

The surface energy density Γ is taken to be a function of the concentration C, the concentration gradient $C_{,\alpha}$, and the strain in the surface, $\varepsilon_{\alpha\beta}$. Greek subscripts run from 1 to 2. Expand the surface energy density to the leading order power series in the concentration gradient and the strain, and we have

$$\Gamma = g(C) + h(C)C_{,\beta}C_{,\beta} + f_{\alpha\beta}(C)\varepsilon_{\alpha\beta}. \tag{5}$$

The leading term in the concentration gradient is quadratic, because the symmetry excludes the term linear in the concentration gradient. We assume that $h(C)=h_0$, a positive constant. The surface stress $f_{\alpha\beta}$ is the excess work per unit area done when the surface enlarges per unit strain. As mentioned before, we assume that $\Delta f_{\alpha\beta} = \phi_{\alpha\beta}\Delta C$.

When the concentration field is uniform, the surface stress is also uniform. Because the substrate is a semi-infinite elastic field, the uniform surface stress induces no elastic field in the substrate. Under these conditions, only $g(C)$ remains in Eq. (5). Consequently, the term $g(C)$ represents the free energy of mixing. We assume that the monolayer is a binary regular solution, so that

$$g(C) = g_\mathrm{A}(1-C) + g_\mathrm{B}C + \Lambda k_\mathrm{B}T[C\ln C + (1-C)\ln(1-C) + \Omega C(1-C)]. \tag{6}$$

Here g_A and g_B are the excess energy when the monolayer is pure A and pure B. When the average concentration is fixed, g_A and g_B do not affect the free energy change. Λ is the number of atoms per unit area on the surface, k_B is Boltzmann's constant and T is the Kelvin temperature. The dimensionless number Ω measures the mixing enthalpy relative to the mixing entropy. The value adopted in the simulation is Ω=2.2, so that $g(C)$ has double wells at $C_\alpha\approx 0.25$ and $C_\beta\approx 0.75$, corresponding to two phases (Fig. 1b).

The variation of the free energy has three parts: the variation with the elastic displacement, with the concentration, and with λ. Write

$$\delta G = \int \sigma_\mathrm{ij}\delta u_\mathrm{i,j}\mathrm{d}V + \int f_{\alpha\beta}\delta u_{\alpha,\beta}\mathrm{d}A + \int\left(\frac{\partial g}{\partial C} - 2h_0C_{,\beta\beta} + \phi_{\alpha\beta}\varepsilon_{\alpha\beta} - \lambda\right)\delta C\mathrm{d}A - \delta\lambda\int(C \tag{7}$$

$-C_0)\mathrm{d}A$.

We have discarded the integrals along lines on the surface upon using the periodical boundary conditions. The system attains thermodynamic equilibrium when δG=0 for any arbitrary δu_i, δC and $\delta\lambda$.

The free energy variation associated with the elastic displacement variation vanishes, leading to

$$\int \sigma_{ij}\delta u_{i,j}\mathrm{d}V + \int f_{\alpha\beta}\delta u_{\alpha,\beta}\mathrm{d}A = 0. \tag{8}$$

The functional calculus gives the field equation inside the substrate:

$$\sigma_{ij,j} = 0, \tag{9}$$

and the traction vector on the surface of the substrate:

$$\sigma_{3\alpha} = \phi_{\alpha\beta}C,_{\beta}, \tag{10}$$

and σ_{33}=0. Consequently, mechanical equilibrium defines an elasticity boundary value problem in the semi-infinite solid with prescribed surface traction.

The free energy variation associated with the variation in the concentration vanishes, leading to

$$\lambda = \frac{\partial g}{\partial C} - 2h_0C,_{\beta\beta} + \phi_{\alpha\beta}\varepsilon_{\alpha\beta}, \tag{11}$$

which shows that the Lagrangian multiplier is the chemical potential.

The free energy variation with λ vanishes, leading to

$$\int (C-C_0)\mathrm{d}A = 0, \tag{12}$$

which requires that the average concentration remains constant.

For a given concentration field, mechanical equilibrium is attained by solving the elasticity boundary value problem defined above. The mechanical equilibrium conditions, in conjunction with the divergence theorem, allow us to rewrite the free energy as

$$G = \int\left(g + h_0C_{,\alpha}C_{,\alpha} - \frac{1}{2}\sigma_{3\alpha}u_\alpha\right)\mathrm{d}A - \lambda\int(C \tag{13}$$

$-C_0)\mathrm{d}A$.

The integral extends over the entire substrate surface. To determine the equilibrium concentration field, we will minimize the free energy (13), rather than use the condition of constant chemical potential (11).

Following [14,15], we introduce two length scales. The comparison of the free energy of mixing and the phase boundary energy defines a length scale

$$b = \left(\frac{h_0}{\Lambda k_B T}\right)^{1/2}, \tag{14}$$

which is approximately the width of the phase boundary. The magnitude of h_0 is of the order of energy per atom at the phase boundary. Using magnitudes h_0~10^{-19}J, Λ~5×10^{19} m^{-2} and T~400 K, we obtain that b~0.6 nm.

A comparison of the phase boundary energy and the elastic energy determines another length scale

$$l = \frac{2\mu h_0}{(1-\nu)\phi_1{}^2}, \tag{15}$$

where ϕ_1 is the larger principal component of the $\phi_{\alpha\beta}$ tensor. According to [3], the surface stress slope tensor is about ϕ_1~4 N/m. Young's modulus is about E~10^{11} N/m^2. With those estimates, we get l~0.6 nm. As we will see later, the width of a stripe is on the order of 10 l.

3. Parallel stripes under isotropic surface stress

In this section, the concentration field is constrained to vary in one direction, corresponding to an array of periodic, parallel stripes. The surface stress is taken to be isotropic, so that $\phi_{11}=\phi_{22}=\phi_1$, and ϕ_{12}=0. The purpose of this section is to illustrate the method. In reality, the stripes may line up in a particular orientation because, say, the phase boundary energy in the orientation is the smallest.

Denote the direction in which the concentration varies by x_1, and the period by $2\pi/\kappa$. Represent the periodic concentration field by a Fourier series:

$$C = C_0 + \sum q_n\cos(n\kappa x_1). \tag{16}$$

The summation runs from n=1 to n=∞. The cosine

series (16) eliminates the translational symmetry of the system, and ensures that the average concentration is C_0. We seek the wavenumber κ and the coefficients q_n to minimize the free energy. Incidentally, Lu and Suo [12] used a single sinusoidal mode in the linear stability analysis. As we will see later, the single mode concentration field can be significantly different from the equilibrium concentration field.

The free energy per unit area is calculated by the free energy in a period divided by the wavelength. The energy of mixing per unit area is

$$\frac{\kappa}{2\pi}\int_{(-\pi/\kappa)}^{(\pi/\kappa)} g(C)\mathrm{d}x_1 = L\Lambda k_\mathrm{B}T, \tag{17}$$

where

$$L = \frac{1}{2\pi}\int_{-\pi}^{\pi} [C1\mathrm{n}C + (1-C)1\mathrm{n}(1-C) + \Omega C(1-C)]\mathrm{d}\alpha, \tag{18}$$

with $\alpha=\kappa x_1$. This integral is carried out by numerical quadrature.

The gradient energy per unit area is

$$\frac{\kappa}{2\pi}\int_{-\pi/\kappa}^{\pi/\kappa} h_0\left(\frac{\partial C}{\partial x_1}\right)^2 \mathrm{d}x_1 = \frac{1}{2}Sh_0\kappa^2, \tag{19}$$

where

$$S = \sum n^2 q_n^2. \tag{20}$$

We now calculate the elastic energy. A combination of Eqs. (10) and (16) gives the traction components on the substrate surface:

$$\sigma_{31} = -\kappa\phi_1\sum nq_n\sin(n\kappa x_1),\ \sigma_{32} = 0,\ \sigma_{33} = 0. \tag{21}$$

The semi-infinite substrate is in a state of plane strain elastic deformation in the plane (x_1,x_3). The displacement field is periodic in x_1, and decays exponentially in x_3. The elasticity boundary value problem can be solved analytically [20]. Specifically, the solution gives the displacements on the substrate surface:

$$u_1 = -\frac{(1-\nu)\phi_1}{\mu}\sum q_n\sin(n\kappa x_1),\ u_2 = 0. \tag{22}$$

The elastic work per unit area is

$$\frac{\kappa}{2\pi}\int_{-\pi/\kappa}^{\pi/\kappa}\frac{1}{2}\sigma_{3\alpha}u_\alpha \mathrm{d}x_1 = \frac{{\phi_1}^2(1-\nu)}{4\mu}Q\kappa, \tag{23}$$

where

$$Q = \sum nq_n^2. \tag{24}$$

From Eq. (13), the total free energy per unit area is

$$G = L\Lambda k_\mathrm{B}T + \frac{1}{2}Sh_0\kappa^2 - \frac{{\phi_1}^2(1-\nu)}{4\mu}Q\kappa. \tag{25}$$

The dimensionless factors L, S and Q depend on the Fourier coefficients q_n, but not on the wavenumber κ. Consequently, the total free energy is quadratic in the wavenumber. The free energy of mixing is independent of the wavenumber. The phase boundary energy decreases as the wavenumber decreases, and drives the phases to coarsen. The elastic energy decreases as the wavenumber increases, and drives the phases to refine.

The competition between the coarsening and the refining actions determines the equilibrium width of the stripes. Setting $\partial G/\partial\kappa=0$, we obtain the equilibrium wavenumber:

$$\kappa_{\mathrm{eq}} = \frac{Q}{2lS}. \tag{26}$$

When only the $n=1$ term is retained, $S=Q={q_1}^2$, and $\kappa_{\mathrm{eq}} = \frac{1}{2l}$ This agrees with the previous prediction on the basis of the linear perturbation analysis [12]. If the higher frequency terms are retained, the equilibrium wavenumber must be determined after the Fourier coefficients q_1, q_2, q_3… are determined.

Combining Eqs. (25) and (26), we write the free energy in a dimensionless form:

$$\frac{G}{\Lambda k_\mathrm{B}T} = L - \frac{1}{8}\left(\frac{b}{l}\right)^2\frac{Q^2}{S}. \tag{27}$$

The free energy is a function of the Fourier coefficients, q_n. We use the conjugate-gradient method

[21] to seek the energy minimizer. Truncate the Fourier series (16) to a finite number of terms N, and denote q_1, q_2…, q_N as a vector $\mathbf{q}$. Start with an initial guess, $\mathbf{q}_0$, and update iteratively. At $\mathbf{q}_i$, locate $\mathbf{q}_{i+1}$ along a certain direction in the $\mathbf{q}$-space by minimizing the energy as a function of a single variable. The conjugate-gradient method prescribes an algorithm for the direction at each iteration.

One serious issue is how to make the initial guess. As mentioned before, the cosine series (16) eliminates the translational symmetry. However, one can readily see that several other symmetries leading to multiple minimizers. For example, the location $x_1=0$ can correspond to either the high-concentration phase or the low-concentration phase. As our formulation stands, within the period $2\pi/\kappa$, one can fit one concentration wave, or any number of concentration waves. We can eliminate the multiplicity by starting at $q_1=+0.4$ (say), $q_2=q_3=\ldots=0$.

We first keep $C_0=0.5$ and vary b/l in the numerical calculation. Fig. 3a shows the equilibrium concentration field for $b/l=1.0$. We use 12 terms in the Fourier series to attain convergence. The equilibrium concentration field is more like a rectangular wave than a sinusoidal wave. The sinusoidal curve with wavelength $4\pi l$ is obtained by energy minimization with only 1 term in the Fourier series. The difference in the two curves shows that the linear perturbation analysis is inadequate to predict the equilibrium state of the nonlinear system. Fig. 3b shows the equilibrium concentration field for $b/l=0.5$. We find that in this case 24 terms are needed to achieve convergence. The difference between 24-terms and 1-term energy minimization is quite large. Fig. 3c shows the equilibrium concentration field for $b/l=1/3$. In this case, 50 terms are needed to achieve convergence. The difference between 1 term and 50 terms energy minimization is very large indeed. In all three cases note that the peak and bottom concentrations deviate significantly from those predicted by two valleys of the function $g(C)$. This is because the equilibrium concentration field minimizes the combined free energy of mixing, phase boundary and elasticity, not just $g(C)$. The deviation is pronounced when b/l is large, and lessens when b/l is small.

It is an interesting hindsight that if the kinetic

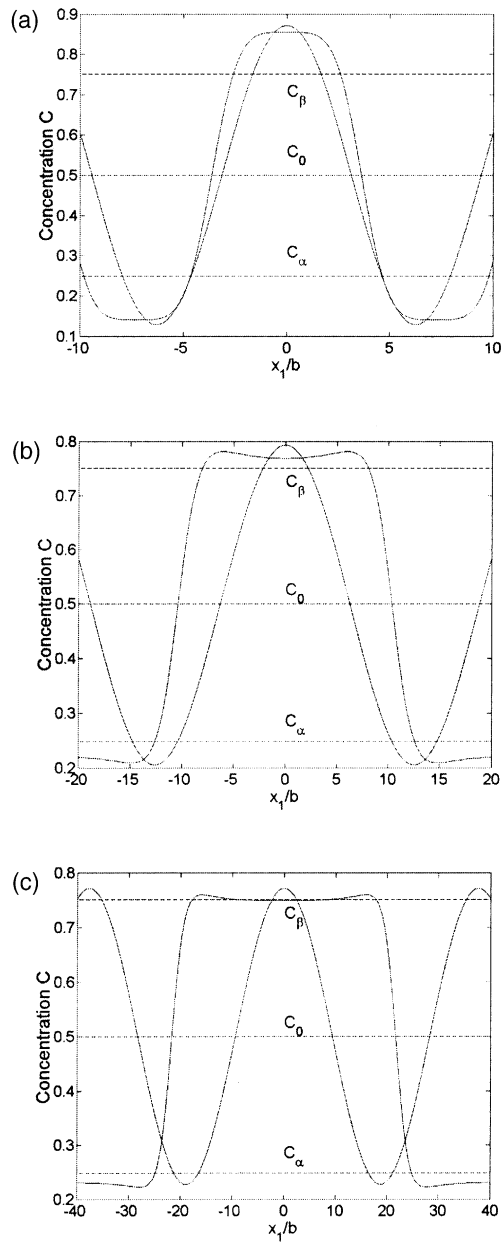

Fig. 3. Equilibrium concentration field ($C_0=0.5$). (a) The rectangle-like wave is calculated by using a 12 term Fourier series, and the sinusoidal wave is with only 1 term. The parameter is $b/l=1.0$. (b) Similar calculation for $b/l=0.5$. (c) Similar calculation for $b/l=1/3$.

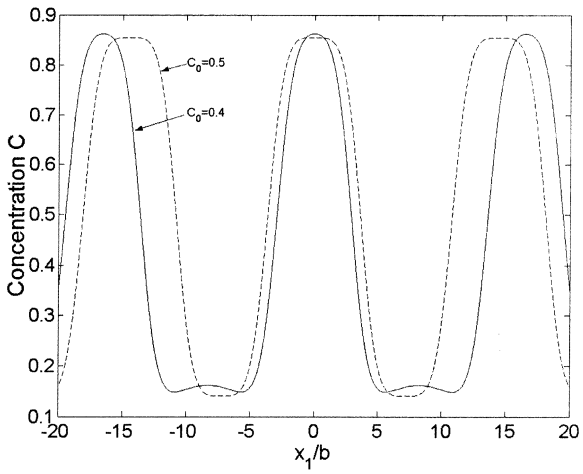

Fig. 4. Equilibrium concentration profile with b/l=1.0, for average concentration C_0=0.4 and C_0=0.5.

simulation is carried out in a cell smaller than even $4\pi l$, the phases only coarsen, as shown in [13]. At that time, we did not appreciate the significance of $4\pi l$, and were disappointed that our model did not produce the stable patterns.

We next keep b/l=1.0 and vary C_0 (restricted between C_α and C_β). Fig. 4 compares the equilibrium concentration fields for C_0=0.4 and C_0=0.5. For the smaller average concentration, the bottoms become wider, while the peaks become narrower. Fig. 5 shows the free energy and wavenumber at equilibrium as functions of the average concentration. The free energy increases with the decrease of the average concentration, while the wavenumber decreases. We find that the energetic minimization method can be used in both the spinodal decomposition region, and the nucleation-growth region.

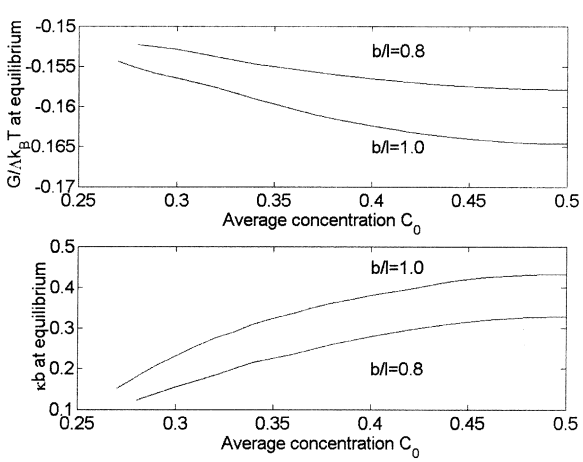

Fig. 5. The free energy and wavenumber at equilibrium as functions of average concentration C_0 (b/l=1.0 and isotropic surface stress).

4. Anisotropic surface stress and stripe orientation

As shown in Fig. 2, when the surface stress tensor is anisotropic, the stripes will select certain orientations to minimize the free energy. The free energy is quadratic in ϕ_1 and ϕ_2, the principal values of the ϕ-tensor. Without loss of generality, assume that $|\phi_2|<|\phi_1|$. Inspecting Eq. (25), one might speculate that the stripes will orient in the ϕ_2 direction to minimize the free energy. As pointed out in [16], this speculation is not always correct. The detailed answer is far more interesting. This section is devoted to a physical explanation of the answer.

Fig. 6 shows the configuration to be analyzed. The concentration field is constrained to form parallel stripes at an angle θ from the ϕ_2 direction. Let

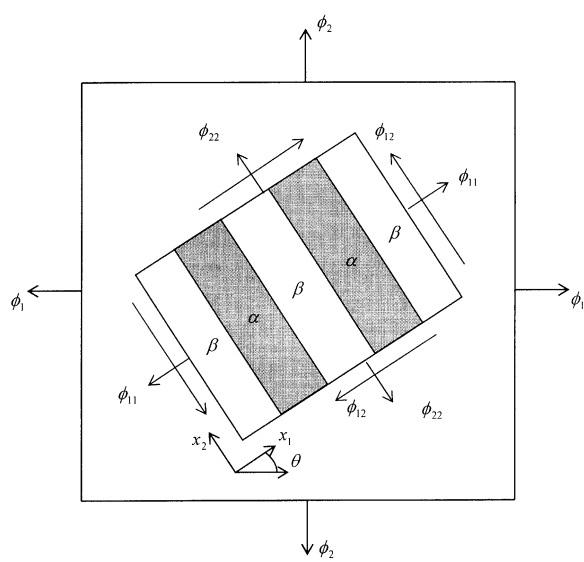

Fig. 6. Geometrical conventions used in the analysis where the surface stress is anisotropic.

x_1 and x_2 coincide with the direction normal and parallel to the stripes. The concentration field is still represented by the Fourier series (16). In calculating the free energy from (13), we find that the energy of mixing and the gradient energy remain the same as in Eq. (25). We next calculate the elastic energy.

In the x_1 and x_2 coordinates, the components of the ϕ-tensor are

$$\phi_{11} = \phi_1\cos^2\theta + \phi_2\sin^2\theta, \tag{28}$$

$$\phi_{12} = (\phi_2 - \phi_1)\sin\theta\cos\theta. \tag{29}$$

When ϕ_1 and ϕ_2 have different signs, a change in θ from zero gives rise to a significant increase in the magnitude of ϕ_{12}, and a decrease in the magnitude of ϕ_{11}. As will become clear, this fact of tensor transformation plays a part in our explanation.

Inserting Eq. (16) into (10), we find that on the substrate surface, the traction has the components

$$\sigma_{31} = -\phi_{11}\kappa\sum nq_n\sin(n\kappa x_1), \tag{30}$$

$$\sigma_{32} = -\phi_{12}\kappa\sum nq_n\sin(n\kappa x_1). \tag{31}$$

Since the modulation of the concentration is along the x_1 direction, inside the substrate, with reference to the plane (x_1,x_3), σ_{31} causes an inplane strain field, and σ_{32} causes an antiplane strain field. Solving the two elasticity boundary value problems separately [20], we obtain the two displacement components on the substrate surface:

$$u_1 = -\frac{(1-\nu)\phi_{11}}{\mu}\sum q_n\sin(n\kappa x_1), \tag{32}$$

$$u_2 = -\frac{\phi_{12}}{\mu}\sum q_n\sin(n\kappa x_1), \tag{33}$$

where u_1 is the inplane deformation caused by σ_{31}, and u_2 is the antiplane deformation caused by σ_{32}. The forms of Eqs. (32) and (33) can be deduced on the basis of linearity and dimensional considerations. The detailed boundary value problems just fix the numerical pre-factors, being 1 on both cases.

The elastic work per unit area is

$$\frac{\kappa}{2\pi}\int_{-\pi/\kappa}^{\pi/\kappa}\frac{1}{2}\sigma_{3\alpha}u_\alpha \mathrm{d}x = \frac{\kappa}{4\mu}Q[(1-\nu)\phi_{11}{}^2 + \phi_{12}{}^2], \tag{34}$$

where Q is the same as in Eq. (24). Remarkably, when $|\phi_{12}| = |\phi_{12}|$, the shear surface stress slope ϕ_{12} makes a larger contribution than the normal surface stress slope ϕ_{11}. Now we can qualitatively understand the transition from the along-axis to the off-axis stripes. When the stripes are along the ϕ_2-axis, θ=0, only ϕ_1 contributes to elastic energy relaxation, and the elastic deformation is inplane. When the stripes are off the ϕ_2-axis, $\theta\neq0$, both ϕ_1 and ϕ_2 contribute to elastic energy relaxation, and the elastic deformation is a combination of inplane and antiplane. When $\theta\neq0$, although the inplane relaxation decreases, the antiplane relaxation can compensate more, provided ϕ_2 is significantly negative.

From Eqs. (13), (25), (28), (29) and (34), the total free energy per unit area is

$$G = L\Lambda k_B T + \frac{1}{2}Sh_0\kappa^2 - \frac{\kappa\phi_1{}^2}{4\mu}Q[(1-\nu) - R(\eta)], \tag{35}$$

where

$$R(\eta) = (1-r)[r + (1-2\nu)]\eta^2 + \nu(1-r)^2\eta^4, \tag{36}$$

and η=sin θ, r=ϕ_2/ϕ_1. We observe again that L, S and Q depend on q_n, but not on the wavenumber κ and the orientation θ. So long as the θ-dependence is concerned, $R(\eta)$ represents the free energy.

Eq. (36) shows that the transition from the along-axis stripes to the off-axis ones follows the Landau theory [22]. So long as $r\neq1$, the coefficient for the η^4 term is always positive. The coefficient for the η^2 term is positive when $r>r_c$, and negative when $r<r_c$, where $r_c=-1+2\nu$. Fig. 7 shows the dependence of R on the angle θ (ν=0.3). Three values of r are selected to show the representative behaviors. When r=1, the surface stress tensor is isotropic, and R=0, so that all orientations are energetically equivalent, as expected. When r=0.2, the minimum of $R(\theta)$ occurs at θ=0, so that the preferred stripe is along ϕ_2 direction. When r=-0.8, $R(\theta)$ has two minima, so that the preferred stripes are off the ϕ_2 direction, and have two variants.

When $r<r_c$, setting $\mathrm{d}R/\mathrm{d}\eta$=0, we obtain the equilibrium orientation of the stripe:

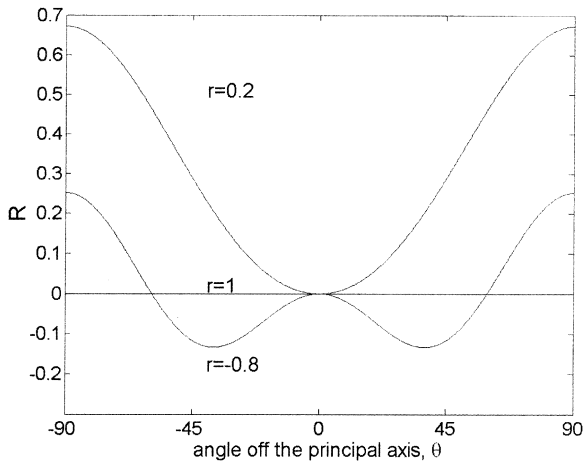

Fig. 7. R as a function of the angle θ. Depending on r, three kinds of behaviors are evident. When r=1, R=0, and stripes of all orientations have identical free energy. When r=0.2, R reaches a minimum at θ=0, and the equilibrium stripes line up in the x_2-direction. When r=0.8, R reaches two minima at some $-\theta$ and $+\theta$, and the equilibrium stripes have two variants, forming $\pm\theta$ angles with respect to the x_2-axis

$$\eta_{eq} = \pm\sqrt{\frac{r_c - r}{2\nu(1-r)}}. \tag{37}$$

For instance, when r=-1.0, the equilibrium angles are $\pi/4$ and $-\pi/4$.

Define a new length scale l' as

$$l' = \frac{l}{1 - R/(1-\nu)}. \tag{38}$$

The equilibrium wavenumber is in the same form as Eq. (26) with the substitution l' for l. Consequently, the surface stress anisotropy determines the stripe orientation, and also alters the equilibrium wavenumber.

5. The herringbone structure and the colonies

When the stripes are off the principal axis of the ϕ-tensor, the stripes can make either a positive or negative angle from the principal axis. By symmetry, the two variants are energy equivalent. Our kinetic simulation has shown that the two variants coexist to form a herringbone pattern (Fig. 2). As pointed out by Narasimhan and Vanderbilt [8], the herringbone forms to further relax the elastic energy. A set of stripes of the same variant from a colony. At a course level, the two kinds of colonies have different homogenized stress states, so that different colonies interact elastically. The transition between the two colonies can be thought of as a domain boundary. Consequently, the competition selects another equilibrium length scale: the size of the colony. Note that the "domain boundary energy" in this context is caused by the elastic interactions and is captured by the factor Q below in our calculation. This section calculates the free energy of the herringbone patterns, and determines the equilibrium size of the individual colony.

Any two-dimensional (2D) periodic pattern can be represented by replicating a rectangular unit cell. Denote the sides of the cell by $2\pi/\kappa_1$ and $2\pi/\kappa_2$. Let $\kappa = \sqrt{\kappa_1^2 + \kappa_2^2}$, $\kappa_1 = h_1\kappa$ and $\kappa_2 = h_2\kappa$. Represent the concentration field by the 2D Fourier series:

$$C(x_1,x_2) = \sum q_{n_1n_2}\exp[i(n_1\kappa_1 x_1 + n_2\kappa_2 x_2)]. \tag{39}$$

The integers n_1 and n_2 run from $-\infty$ to $+\infty$. The constant average concentration requires that $q_{00}=C_0$. The real-valued concentration requires that $q_{(-n_1)(-n_2)} = \bar{q}_{n_1n_2}$ The coordinates x_1 and x_2 are along the principal directions ϕ_1 and ϕ_2.

The total free energy per unit area is still given in the form (25), with

$$L = \frac{1}{(2\pi)^2}\int_{-\pi}^{\pi}\int_{-\pi}^{\pi}[C\ln C + (1-C)\ln(1-C) + \Omega C(1-C)]\mathrm{d}\alpha_1\mathrm{d}\alpha_2, \tag{40}$$

$$S = 2\sum|q_{n_1n_2}|^2(n_1^2h_1^2 + n_2^2h_2^2). \tag{41}$$

$$Q = 2\sum|q_{n_1n_2}|^2\left\{\frac{n_1^2h_1^2 + r^2n_2^2h_2^2}{\sqrt{n_1^2h_1^2 + n_2^2h_2^2}} + \frac{\nu(1-r)^2n_1^2h_1^2n_2^2h_2^2}{1-\nu(n_1^2h_1^2 + n_2^2h_2^2)^{3/2}}\right\}. \tag{42}$$

Here $\alpha_1=\kappa_1x_1$ and $\alpha_2=\kappa_2x_2$. The derivation of Eq. (42) requires the solution of the elasticity problem in the reciprocal space [23]. The magnitude of equilibrium wavevector κ is also given by Eq. (26). The remaining problem is to seek the minima of the free energy (27).

The conjugate-gradient method and many other methods could only lead to local minima [21]. The success of these minimization methods depends sensitively on the initial guess. Furthermore, because the concentration can only be in the interval (0,1), the Fourier coefficients cannot vary freely, which brings additional difficulty to the energy minimization algorithm. We are unable to find the global minimum by starting from a random initial guess. Because our kinetic simulation has shown that stripes and herringbones are possible patterns, we decide to compare the free energies of herringbone structures with various colony sizes.

Fig. 8 depicts two types of possible herringbone structures, denoted as type-X and type-Y, respectively. Calculations in this section assume b/l=1.0 and C_0=0.5. Fig. 9 draws the free energy as a function of the colony size. There indeed exists an energy valley, corresponding to a stable colony size. When r=−1.0, type-X and type-Y are equivalent. The energy valley corresponds to a colony size around 30b, while the size for one stripe is around 12b. The free energy of the herringbone structure is around 10% lower than the uniform off-axis stripes. For r=−0.6, we calculated the two kinds of possible herringbone structures. The energetically favored configuration is the type-Y herringbones. The equilibrium colony size becomes larger than that for r=−1.0. This trend is also evident in Fig. 1(d) and (e).

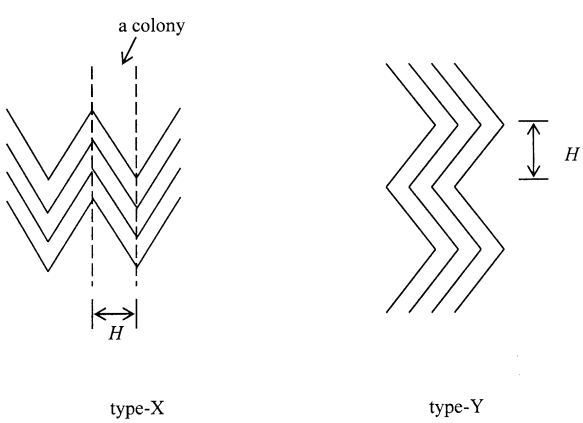

Fig. 8. Two types of herringbone structures, X and Y. The individual colony size is H.

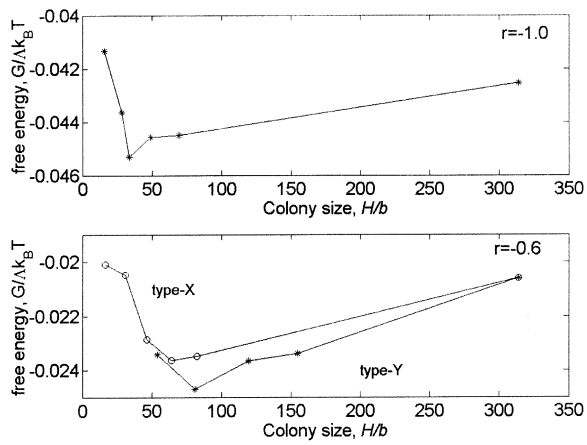

Fig. 9. Free energy as a function of the colony size H.

6. Conclusion

On a solid surface, a two-phase monolayer self-assembles into various patterns. We formulate a free energy model, and adopt the conjugate-gradient method to seek the equilibrium phase patterns. For parallel stripes, the equilibrium concentration profile is like a rectangular wave. When the surface stress tensor is anisotropic, the stripes can be along or off the principal axis of the surface stress slope tensor. The formation of the off-axis stripes compromises the inplane and antiplane deformation. The transition between the along-axis stripes to off-axis stripes follows the Landau theory. The two possible off-axis stripes can form a coarse-level herringbone structure. Our 2D simulation confirms that an equilibrium colony size exists.

Acknowledgements

This work is supported by the Department of Energy through contract DE-FG02-99ER45787. Discussions with D.J. Srolovitz and Weinan E are helpful.

References

[1] Kern D, Niehus H, Schatz A, Zeppenfeld P, George J, Comsa G. Phys Rev Lett 1991;67:855.

[2] Zeppenfield PA, Krzyzowski MA, Romainczyk Ch, David R, Comsa G, Röder H, Bromann K, Brune H, Kern K. Surf Sci 1995;342:L1131.
[3] Ibah H. Surf Sci Rep 1997;29:193.
[4] Pohl K, Bartelt MC, de la Figuera J, Bartelt NC, Hrbek J, Hwang RQ. Nature 1999;397:238.
[5] Plass R, Last JA, Bartelt NC, Kellogg GL. Nature 2001;412:875.
[6] Ellmer H, Repain V, Rousset S, Croset B, Sotto M, Zeppenfeld P. Surf Sci 2001;476:95.
[7] Alerhand OL, Vanderbilt D, Meade RD, Joannopoulos JD. Phys Rev Lett 1988;61:1973.
[8] Narasimhan S, Vanderbilt D. Phys Rev Lett 1992;69:1564.
[9] Ng K-O, Vanderbilt D. Phys Rev B 1995;52:2177.
[10] Vanderbilt D. Surf Rev Lett 1997;4:811.
[11] Suo Z, Lu W. J Mech Phys Solids 2000;48:211.
[12] Lu W, Suo Z. Zeitschrift fur Metallkunde 1999;90:956.
[13] Suo Z, Lu W, In: Chuang, T-J, Rudnick, JW, editors., Multi-scale deformation and fracture in materials and structures — The James R. Rice 60th Anniversary Volume, The Netherlands: Kluwer Academic Publishers, 2000. p. 107-122.
[14] Lu W, Suo Z. J Mech Phys Solids 2001;49:1937.
[15] Suo Z, Lu W. J Nanoparticales Res 2000;2:333.
[16] Lu, W, Suo, Z, Phy Rev B. (in press).
[17] Gao, YF, Suo, Z, J Appl Mech. (in press).
[18] Cahn JW, Hilliar JE. J Chem Phys 1958;28:258.
[19] Chen LQ, Wang Y. JOM 1996;48:13.
[20] Timoshenko SP, Goodier JN. Theory of elasticity. New York: McGraw-Hill, 1970.
[21] Press WH, Teukolsky SA, Vetterling WT, Flannery GP. Numerical recipes in C: the art of scientific computing 2nd ed. In: UK, Cambridge University Press, 1992.
[22] Landau LD, Lifshitz EM. Statistical physics, Part I. Oxford, UK: Butterworth Heinemann, 1980.
[23] Gao, YF, Suo, Z, (in preparation).